International Journal of Greenhouse Gas Control 110 (2021) 103431

Contents lists available at ScienceDirect

International Journal of Greenhouse Gas Control

journal homepage: www.elsevier.com/locate/ijggc

Process optimization of a fixed bed reactor system for direct air capture

H.M. Schellevis *, T.N. van Schagen, D.W.F. Brilman

University of Twente, Faculty of Science and Technology, PO Box 217, Enschede 7500AE, The Netherlands

ARTICLE INFO

Keywords:
Direct air capture
Adsorption
Supported-amine sorbents
Process optimization
Dynamic modelling

ABSTRACT

The extraction of CO_2 directly from the atmosphere (Direct Air Capture) is commonly employed using supported-amine sorbents. This adsorption technology is under rapid development with novel sorbent materials emerging and with processes being demonstrated on increasingly larger scale. Optimization of such processes requires accurate knowledge on sorbent characteristics and knowledge on how operational variables affect process performance. This study primarily focuses on the latter, where we aim to quantify the influence of operational parameters on the energy duty and CO_2 productivity. In addition, we examine the influence of weather conditions on the adsorption rate. For this, we develop a dynamic model of the complete temperature-vacuum swing adsorption cycle (TVSA). This model was validated by experimental results on a kg-scale direct air capture system. The impact of selected operational variables was assessed by two-dimensional sensitivity analyses. We show that desorption temperature is preferably high, limited by the chemical stability of the sorbent material in this particular case. In addition, the sorbent working capacity should be high when opting for an optimization towards energy duty, whereas it reaches a clear optimum in terms of CO_2 productivity. Finally, we conclude that weather conditions and diurnal variations can significantly affect the performance of a direct air capture process and should certainly be considered during design and operation. With these insights and the developed model, this study provides a sound basis for further process development and optimization of direct air capture using fixed bed technology combined with solid amine sorbents.

1. Introduction

Direct Air Capture (DAC), the extraction of CO_2 directly from the atmosphere, is considered an important technology in climate change mitigation (Breyer et al., 2019; Lackner et al., 2012; Beuttler et al., 2019). Rogelj et al. (2015) identified carbon neutrality by the year 2050 as an essential aspect to limit the temperature rise to 1.5°C. DAC is a technology that enables zero or negative emission technologies, because a sustainable carbon source is acquired. These carbon sources are necessary to produce limitless products, food, feed and materials of our everyday life (Speight, 2011). CO_2 as carbon source requires alternative production routes towards these products (Peters et al., 2011; Lim, 2015), for example via chemical reduction with H_2 to form methanol (Bos et al., 2020) or via cultivation of microalgae and subsequent biorefining (Wijffels et al., 2010).

In 1999, Lackner et al. (1999) were the first to propose DAC as viable option to reduce CO_2 emissions. Nowadays, two major technologies are considered for DAC on commercial scale: absorption using alkaline solutions and adsorption using amine-functionalized solid sorbents (Keith et al., 2018; Zeman, 2007; Socolow, 2011; Gebald et al., 2011; Fasihi et al., 2019; Goeppert et al., 2012; Bajamundi et al., 2019). Absorption with alkaline solutions was the proposed technology by Lackner et al. (1999). Keith et al. (2018) used this concept to develop an industrial scale process in which aqueous KOH is the capture medium and a calcium caustic loop is used to recover CO_2. Adsorption using amine-functionalized sorbents is the second major DAC technology in which CO_2 reacts with amine-groups on the internal surface of the sorbent. The CO_2 is then recovered by a temperature and/or vacuum swing (Elfving et al., 2021; Bos et al., 2019b). Sorbent development is dominating research efforts in this research area (Choi et al., 2009; D'Alessandro et al., 2010; Gelles et al., 2020; Sanz-Pérez et al., 2016; Singh et al., 2020).

The number of studies for DAC on contactor and process scale is limited. However, quantification of the influence of operating parameters on DAC performance is highly desired, since this will pinpoint the opportunities for process improvement, either by process optimization or sorbent optimization (Stampi-Bombelli et al., 2020). This is a complex endeavor since many operational parameters are involved within the whole temperature-vacuum swing adsorption cycle.

* Corresponding author.
E-mail address: h.m.schellevis@utwente.nl (H.M. Schellevis).

https://doi.org/10.1016/j.ijggc.2021.103431
Received 11 May 2021; Received in revised form 29 July 2021; Accepted 8 August 2021
Available online 21 August 2021

Nomenclature

ΔH_0	Tóth heat of adsorption (J mol^{-1})
$\Delta_c H$	difference in enthalpy between monolayer and multilayer (J mol^{-1})
$\Delta_k H$	difference in enthalpy between bulk liquid and multilayer (J mol^{-1})
$\Delta_r H_i$	reaction heat of component i (J mol^{-1})
a_s	specific surface area (m^2 m$_r^{-3}$)
b	Tóth affinity constant (Pa^{-1})
b_0	Tóth affinity constant at reference temperature (Pa^{-1})
C_0	Arrhenius pre-exponential factor for C_G (–)
C_G	Guggenheim constant in GAB isotherm (–)
C_m	monolayer capacity in GAB isotherm (mol kg^{-1})
C_p	specific heat capacity (J kg^{-1} K^{-1})
c	concentration (mol m^{-3})
D_{ax}	axial dispersion coefficient (m^2 s^{-1})
E_{act}	activation energy (J mol^{-1})
h_t	heat transfer coefficient (W m^{-2} K^{-1})
K_{ads}	multilayer correction factor in GAB isotherm (–)
K_0	Arrhenius pre-exponential factor for K_{ads} (–)
k_0	Arrhenius pre-exponential factor for reaction rate (s^{-1} or mol kg$_s^{-1}$ bar^{-1} s^{-1})
k_{LDF}	linear driving force reaction rate constant (s^{-1})
k_T	Tóth reaction rate constant (mol kg$_s^{-1}$ bar^{-1} s^{-1})
p	pressure (Pa)
q	sorbent loading (mol kg$_s$ $^{-1}$)
q_s	Tóth maximum capacity (mol kg$_s$ $^{-1}$)
$q_{s,0}$	Tóth maximum capacity at reference temperature (mol kg$_s^{-1}$)
R	ideal gas constant (J mol^{-1} K^{-1})
R_i	reaction rate of component i (mol kg$_s^{-1}$ s^{-1})
T	temperature (K)
T_0	Tóth reference temperature (K)
t	time (s)
t_h	Tóth heterogeneity constant (–)
$t_{h,0}$	Tóth heterogeneity constant at reference temperature (–)
u	superficial gas velocity (m$_g^3$ m$_r^{-2}$ s^{-1})
z	axial direction (m)

Greek symbols

α	temperature dependency parameter of t_h (–)
δ	identification of energy point source in 1D model (–)
E	void fraction (m$_g^3$ m$_r^{-3}$)
η	effectiveness factor (–)
λ_{ax}	axial thermal conductivity (W m^{-1} K^{-1})
ρ	density (kg m^{-3})
χ	temperature dependency parameter of q_s (–)
Φ	gas flow rate (NL min^{-1})

Subscripts

CO_2	carbon dioxide
g	gas phase
H_2O	water
i	components
r	reactor
s	solid phase

Table 1
Physical properties of the solid amine sorbent.

Parameter	Value	Ref
$\varepsilon_p(-)$	0.23	(Veneman et al., 2012)
$C_{p,s}(J/(molK))$	1580	(Sonnleitner et al., 2018)
$\rho_s(kg/m^3)$	880	(Veneman et al., 2012)
$\lambda_{ax}(W/(mK))$	0.121	(Bos et al., 2019)
$\Delta_r H_{CO_2}(kJ/mol)$	75	(Sonnleitner et al., 2018)
$\Delta_r H_{H_2O}(kJ/mol)$	43	(Veneman et al., 2015)
$d_p(\mu m)$	668	(Driessen et al., 2020a)

In this study, we aim to find optimal operational parameters of an adsorption based DAC process for a given sorbent and contactor and evaluate this in light of varying weather conditions. Our process uses a multibed, fixed bed technology without sorbent circulation. We develop a detailed dynamic model of the temperature-vacuum swing adsorption process using experimental data on CO_2 and H_2O equilibrium capacity and adsorption kinetics. The effects of selected process parameters are quantified by two-dimensional sensitivity analyses. Finally, we analyze and show the potential effect of varying weather conditions on the performance of a DAC process, an aspect that is often overlooked in DAC design studies.

2. Experimental

2.1. Materials

A commercially available supported-amine sorbent, Lewatit® VP OC 1065 was used in this study. It is a polystyrene polymeric sorbent cross-linked with divinylbenzene. CO_2 adsorption functionality is introduced by primary benzylamine groups. Alesi and Kitchin (2012) determined the concentration of these functional groups at 7.5 mol/kg using energy-dispersive X-ray spectroscopy. Physical properties of this sorbent are listed in Table 1. This sorbent is suitable for CO_2 capture from air as identified in several studies (Bos et al., 2019b; Yu and Brilman, 2020). Important sorbent characteristics for process design are thermal and chemical stability. A sorbent degradation study by (Yu et al., 2017) indicated temperature limits of 150°C (in N_2) to avoid thermal degradation, a limit of 120°C in the presence of CO_2 and a limit of around 70°C in the presence of oxygen.

2.2. CO_2 isotherm measurements

The CO_2 isotherm at low partial pressure was measured via fixed bed breakthrough experiments. This fixed bed has a diameter of 1.3 cm and a length of 60 cm. A water bath (JULABO F32) controls the temperature of the reactor. During a breakthrough experiment, a mixture of N_2 and CO_2 was sent through the reactor, which was loaded with approximately 1.3 g of sorbent. The CO_2 concentration that leaves the reactor was determined with a LI-820 gas analyzer (range: 0 – 20000 ppm). Prior to each breakthrough measurement, the sorbent was completely regenerated with pure N_2 at 80°C. The CO_2 isotherm was determined for a CO_2 partial pressure range of 10 – 100 Pa and a temperature range of 5 – 35°C.

2.3. Kg-scale DAC setup

The aim of this study is the optimization of an adsorption-based fixed bed DAC process. For this, a kg-scale DAC experimental setup was designed. This design of the DAC system is based on design considerations identified in the studies of Yu and Brilman, (2017)) and Schellevis et al. (2020). Fixed bed technology with temperature-vacuum swing adsorption (TVSA) without sorbent circulation is chosen. A series of parallel fixed bed reactors is then required to obtain a

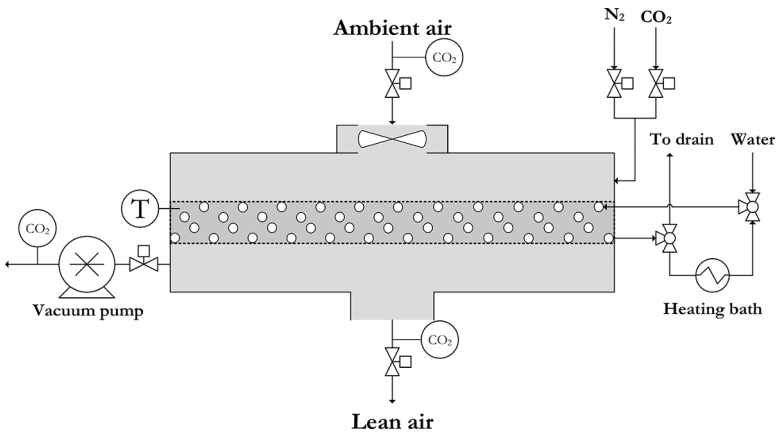

Fig. 1. Experimental setup of a single fixed bed reactor.

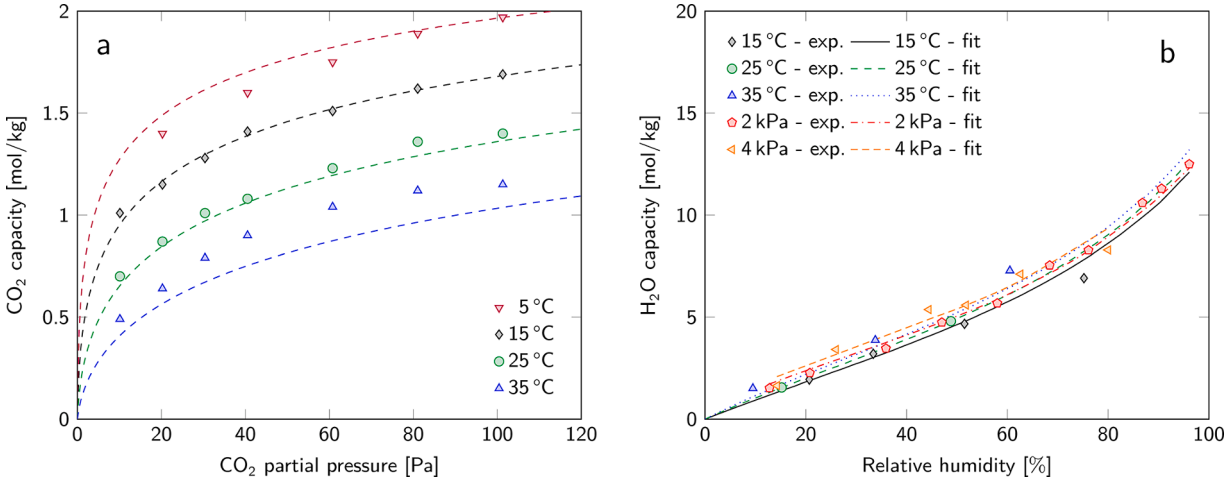

Fig. 2. (a) CO_2 isotherms at low partial pressure under dry conditions, (b) H_2O equilibrium capacity as function of relative humidity for a constant temperature (15 – 35°C) and constant H_2O partial pressure (2 and 4 kPa). Experimental data for the H_2O isotherm are taken from Veneman et al., 2015 and fitted to the GAB model in this work.

semi-continuous production of CO_2. Since model validation is the primary goal of the experimental work on this setup, the experimental setup for this study consist of only one of the four identical fixed bed reactors (Fig. 1). To avoid a large pressure drop, a shallow bed is required and this leads to thin 'flat bed' reactors. In this case, the reactors have a bed thickness of 2.4 cm and a diameter of 40 cm. Heat transfer is accommodated by stacked heating spirals (with a specific heat transfer area of 150 m^2/m^3) using water as cooling and heating medium. These spirals are stacked asymmetrically to avoid preferential flow paths of the gas through the bed. Desorption can be carried out under reduced pressure with air, CO_2, N_2 or a N_2/CO_2 mixture as purge gas. CO_2 concentration is measured in the air inlet (MHZ-16, 0 – 2000 ppm), air outlet (Li-COR 840, 0 – 20,000 ppm) and CO_2 product stream (Sick Maihak, 0 – 15 vol.%). The temperature is measured at nine different locations in the bed by K-type thermocouples. They all have a different distance to a heat source to ensure an accurate average bed temperature.

Adsorption measurements for model validation were performed at ambient conditions for superficial gas velocities of 0.08 – 0.15 m/s. The gas velocity was measured at several locations to make sure that the gas is equally distribution over the cross section of the bed. The valves to the vacuum pump, N_2 and CO_2 were closed and the CO_2 concentration in ambient air and lean air was measured. Adsorption was continued for a certain time or until a certain CO_2 concentration in the lean air was reached. Before each adsorption experiment, the sorbent was completely desorbed.

Desorption measurements for model validation were carried out at atmospheric pressure and reduced pressure (350 mbar). The purge gas flow was varied between 5 and 50 NL/min and was N_2 for all experiments. During desorption, the valves for ambient air and lean air were closed and the N_2 gas flow was controlled by a mass flow controller. Hot water (90°C) was circulated through the heat transfer spirals. The CO_2 concentration was measured in the product stream after the vacuum pump. Desorption was continued until a certain desorption time or until a certain CO_2 concentration in the product stream was reached.

3. Modelling

We developed a 1-dimensional, dynamic fixed bed model that describes the adsorption and desorption behaviour of the DAC process. A sound understanding of sorbent characteristics in terms of CO_2 and H_2O equilibrium capacity and reaction kinetics is crucial for an accurate description. Additionally, mass and heat transfer processes on particle level as well as on reactor level are important. For this reason, we use the Thiele modulus approach with the approximation of a uniform loading profile, as proposed by Driessen et al. (2020b). This approach takes particle level processes (internal mass transfer and intrinsic adsorption kinetics) into account without the necessity of evaluating a fully coupled particle-reactor model.

Table 2
Fitting parameters of the Tóth isotherm (Bos et al., 2019a), GAB isotherm and H_2O adsorption kinetics.

	Parameter	Value
Tóth isotherm	$q_{s,0}(mol/kg)$	3.40
	$\chi(-)$	0
	$T_0(K)$	353.15
	$b_0(1/Pa)$	93.0×10^{-5}
	$\Delta H_0(kJ/mol)$	95.3
	$t_0(-)$	0.37
	$\alpha(-)$	0.33
Tóth kinetics	$k_{0,CO_2}(mol/(kg\,bar\,s))$	3.5×10^3
	$E_{act,CO_2}(kJ/mol)$	15.2
GAB isotherm	$C_m(mol/kg)$	5.55
	$C_0(-)$	100
	$K_0(-)$	0.92
	$\Delta_c H(kJ/mol)$	− 8.69
	$\Delta_k H(kJ/mol)$	− 0.82
H_2O kinetics	$k_{0,H_2O}(1/s)$	450
	$E_{act,H_2O}(kJ/mol)$	15.2

3.1. Sorbent characterization

A description of the sorbent equilibrium loading of CO_2 and H_2O as well as kinetic data under DAC conditions is required. The CO_2 equilibrium capacity was evaluated at CO_2 partial pressures from 10 – 100 Pa and in the range of 5 – 35°C (Fig. 2a) using fixed bed breakthrough experiments. The Tóth isotherm model is fitted to the experimental dataset (eqs. (1) - (4)). This empirical equation is an extension of the Freundlich and Sips equation (Duong, 1998). It describes the adsorption behaviour for systems with only monolayer adsorption in both lower and upper partial pressure limits. Note that if $t_h = 1$, the isotherm reduces to the Langmuir isotherm.

Since CO_2 adsorption capacity is described by the Tóth isotherm, also the reaction rate is described with an expression based on the Tóth isotherm (Eq. (5)) (Duong, 1998). This reaction rate equation is completely consistent with the Tóth isotherm description, i.e. the same parameters are used (Table 2). Furthermore, the study of Bos et al. (2019a) showed this reaction rate description is preferred over pseudo-first order and pseudo-second order linear driving force models. Also, we assume ideal gas phase behaviour:$P_{CO2} = RTc$.

$$q_{eq}(p_{CO2}, T) = \frac{q_s b p_{CO2}}{(1 + (b p_{CO2})^{t_h})^{\frac{1}{t_h}}} \tag{1}$$

$$b(T) = b_0 \exp\left(\frac{\Delta H_0}{RT_0}\left(\frac{T_0}{T} - 1\right)\right) \tag{2}$$

$$t_h(T) = t_{h,0} + \alpha\left(1 - \frac{T_0}{T}\right) \tag{3}$$

$$q_s(T) = q_{s,0} \exp\left(\chi\left(1 - \frac{T}{T_0}\right)\right) \tag{4}$$

$$R_{CO2}(c_{CO2}, q, T) = k_T\left(RTc_{CO2}\left(1 - \left(\frac{q}{q_s}\right)^{t_h}\right)^{\frac{1}{t_h}} - \frac{q}{bq_s}\right) \tag{5}$$

Amine based sorbents are known to co-adsorb H_2O. Literature data of H_2O equilibrium capacity on Lewatit® VP OC 1065 (Veneman et al., 2015) (Fig. 2b) is fitted to the Guggenheim-Anderson-de Boer (GAB) model (Eq. (6), Table 2) (Quirijns et al., 2005). The GAB model accounts for monolayer adsorption, multilayer adsorption and pore condensation. Parameters C_G and K_{ads} have an Arrhenius type temperature dependency. There is no information available on the reaction kinetics of H_2O on this sorbent, but breakthrough experiments showed that saturation with H_2O is much faster than saturation with CO_2 (Appendix A). We assume that H_2O adsorption is described by a pseudo-first order linear driving force model as proposed by Glueckauf and Coates (Eq. (7)) (Glueckauf and Coates, 1947). The reaction rate constant, k_{LDF}, follows an Arrhenius-type temperature dependency and the parameters are chosen such, to result in significantly faster H_2O adsorption compared to CO_2 adsorption (Table 2).

$$q_{H_2O}(RH) = C_m \frac{C_G K_{ads} RH}{(1 - K_{ads} RH)(1 + (C_G - 1) K_{ads} RH)} \tag{6}$$

$$R_{H_2O}(q, RH) = k_{LDF} RH (q_{eq} - q) \tag{7}$$

3.2. Fixed bed model

A transient adsorption model is developed which describes the complete temperature-vacuum swing adsorption cycle. The cycle consists of separate phases for adsorption, heating, desorption and cooling. These adsorption-desorption cycles are simulated until a cyclic steady-state is achieved.

For the adsorption phase we assume:

- No external mass transfer limitations, since the difference between surface and bulk concentration was found to be negligible;
- Thermal equilibrium between gas and solid phase;
- No radial concentration and temperature profile;
- Constant temperature of heat transfer medium;
- And a constant gas velocity, considering the low CO_2 concentration in the feed.

With these assumptions, the component mass balance becomes:

$$\varepsilon_r \frac{\partial c_i}{\partial t} = \frac{\partial}{\partial z}\left(D_{ax,i}\frac{\partial c_i}{\partial z} - u_g c_i\right) - (1 - \varepsilon_r)\rho_s \frac{\partial q_i}{\partial t} \tag{8}$$

The intrinsic reaction rate equation (Eq. (5)) does not account for internal mass transfer limitations. For this, we use the Thiele modulus approach. The Thiele modulus is a classical concept originally derived for heterogeneous catalytic processes (Thiele, 1939; Froment et al.,

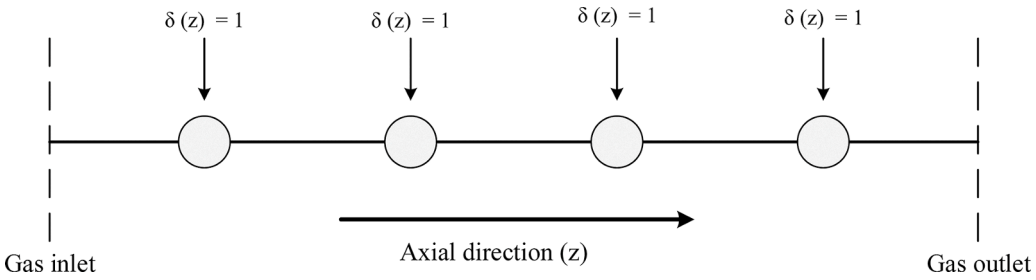

Fig. 3. Placement of heat sources in 1D domain. These are placed at several locations along the axial direction indicated with the grey circles. The distance between the heat sources depends on the average distance to a heat transfer surface in the experimental setup.

Table 3
Model parameters for simulations of adsorption and desorption. These are used in all simulations unless noted otherwise.

	Parameter	Value
Adsorption	$u_g(m/s)$	0.10
	$T(^\circ C)$	20
	$P_{CO_2}(Pa)$	41
	$RH(\%)$	50
	$q_0(mol/kg)$	0.2
Desorption	$T(^\circ C)$	90
	$P(mbar)$	350
	$\phi_{purge}(NL/\text{min})$	15
	Purge gas	N_2

2011). It describes the competition between mass transport and reaction inside a porous particle. Recently, Driessen et al. (2020b) extended this concept to non-equilibrium adsorption processes. The effectiveness factor, η_i, is an essential parameter in this concept, which is defined as the observed adsorption rate including intraparticle transport limitations divided by the adsorption rate at gas bulk concentration and average sorbent loading (Eq. (9)). Using the Thiele modulus approach, the effectiveness factor can be described by an analytical expression using the Thiele modulus at gas phase conditions and average sorbent loading. Consequently, Eq. (10) shows the equation for the adsorption rate as implemented in the mass balances. This approach is only valid for CO_2 adsorption; for H_2O adsorption, the effectiveness factor is assumed to be unity.

$$\eta_i = \frac{\int\int\int R_i(c,q)dV}{R_i(c_b,q_{av})} \tag{9}$$

$$\frac{\partial q_i}{\partial t} = R_i\eta_i \tag{10}$$

Spirals for heating and cooling, with heat transfer medium inside, are located in the sorbent bed perpendicular to the gas flow. This causes non-uniform heating in radial and axial direction. In addition, there is a nonlinear relation between temperature and both equilibrium loading and reaction rate. This leads to sorbent loading gradients based on the heat transfer distance to the heating coils. A uniform energy source in a 1D model would not account for this effect. Therefore, we place point sources for thermal energy along the axial direction of the 1D model based on the average heat transfer distance to the nearest heating coil in the experimental setup (Fig. 3). In the energy balance (Eq. (11)), $\delta(z) = 1$ at the point source and $\delta(z) = 0$ at all other points in the axial domain. To implement this, the domain is discretized in the spatial direction (finite volume) and the heat sources are present in only these designated cells. The time dependency is solved with the ODE solver in MATLAB.

$$\left((1-\varepsilon_r)\rho_s C_{p,s} + \varepsilon_r\rho_g C_{p,g}\right)\frac{\partial T}{\partial t} = \frac{\partial}{\partial z}\left(\lambda_{ax}\frac{\partial T}{\partial z} - u_g\rho_g C_{p,g}T\right) + (1-\varepsilon_r)\rho_s\sum_{i=1}^{n}\Delta_r H_i\frac{\partial q_i}{\partial t} + \delta(z)a_s h_t(T_{ht}-T) \tag{11}$$

Desorption of H_2O and CO_2 causes either the pressure to rise or the gas velocity to increase. We assume the pressure to be constant, since the pressure drop is negligible compared to the total pressure, also during desorption at reduced pressure. Therefore, the gas velocity is not a constant and the overall mass balance is required to account for this (Eq. (12)).

$$\varepsilon_r\frac{\partial c}{\partial t} = \frac{\partial(uc)}{\partial z} + (1-\varepsilon_r)\rho_s\sum_{i=1}^{n}\frac{\partial q_i}{\partial t} \tag{12}$$

Model parameters for the adsorption and desorption are listed in Table 3. These parameters are used in all simulations, unless noted otherwise. Initial conditions are a uniform temperature, concentration and loading profile for simulations of a single phase. For cyclic simulations, the initial conditions are the final profiles of the previous phase. Danckwerts boundary conditions are assumed at the feed inlet and all gradients vanish at the end of the reactor.

Model results are quantified by two key performance indicators (KPIs): daily productivity of CO_2 (in kg_{CO2}/d) and the specific energy duty (in MJ/kg_{CO2}). Energy duty refers to the total energy duty which comprises of: reaction heat of CO_2 and H_2O, sensible heat of sorbent and reactor, sensible heat of purge gas, feed compression and vacuum compression. The total energy duty is used as KPI, which does not discriminate between electrical energy and thermal energy. To account for the thermodynamic difference between these two types of energy input, the fraction of both types will also be considered in the analyses.

4. Results and discussion

4.1. Model validation

The fixed bed model is validated with experimental results. Breakthrough behaviour is the crucial and characteristic aspect of the adsorption phase. Model and experimental results of an adsorption experiment at a superficial gas velocity of 0.15 m/s are shown in Fig. 4a. Immediate breakthrough occurs due to the very short contact time of air

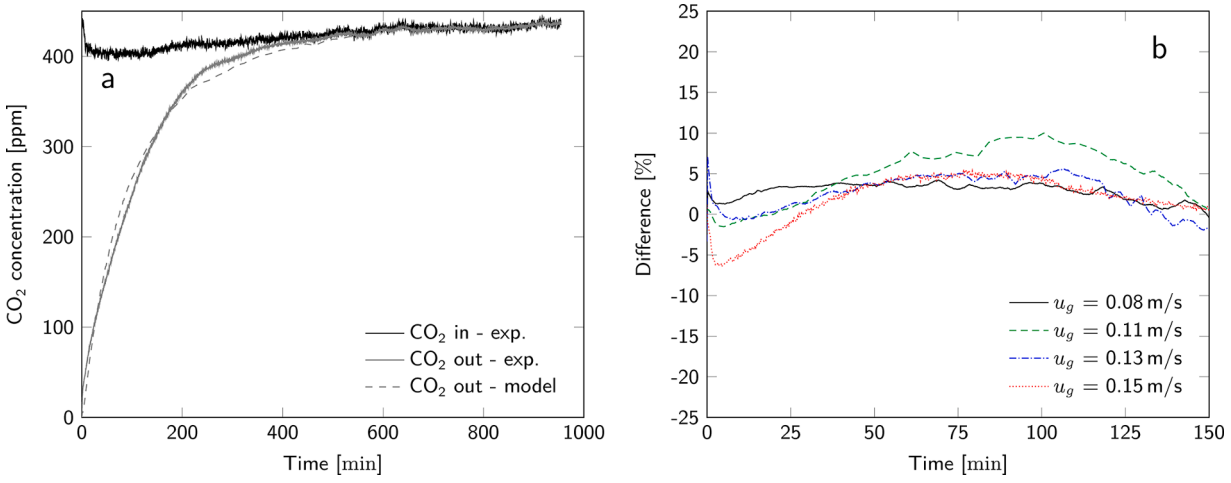

Fig. 4. Model validation for adsorption with (a) the outlet CO_2 concentration of the adsorption breakthrough experiment at 0.15 m/s and (b) the difference between experimental results and model simulations for experiments at different superficial gas velocities.

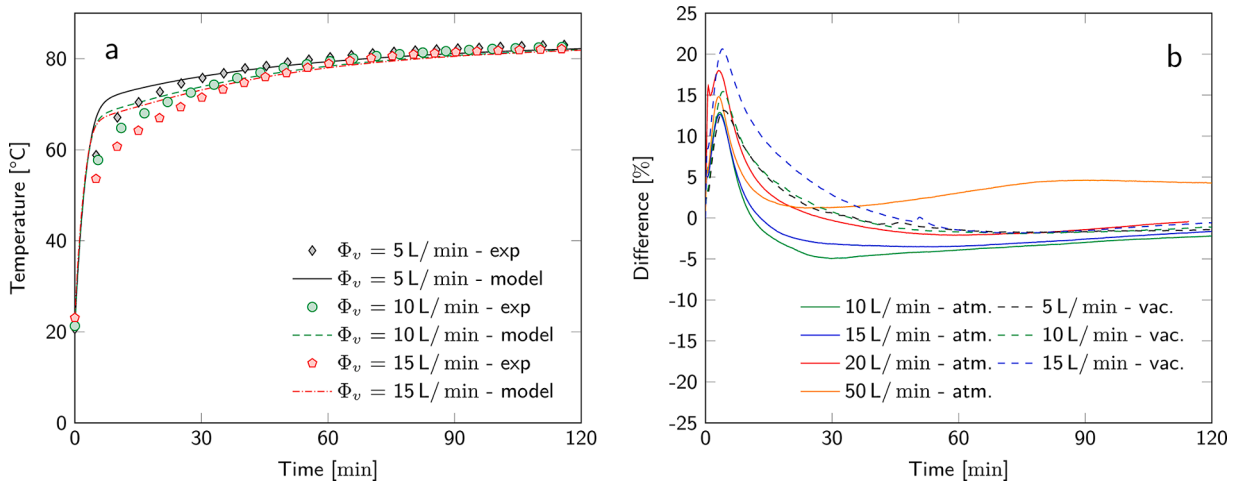

Fig. 5. Model validation for desorption with (a) the desorption temperature over time during desorption with N_2 at reduced pressure for multiple purge gas flow rates and (b) the difference between experimental results and model simulations for atmospheric desorption (atm.) and vacuum desorption (vac.) at multiple purge gas flow rates.

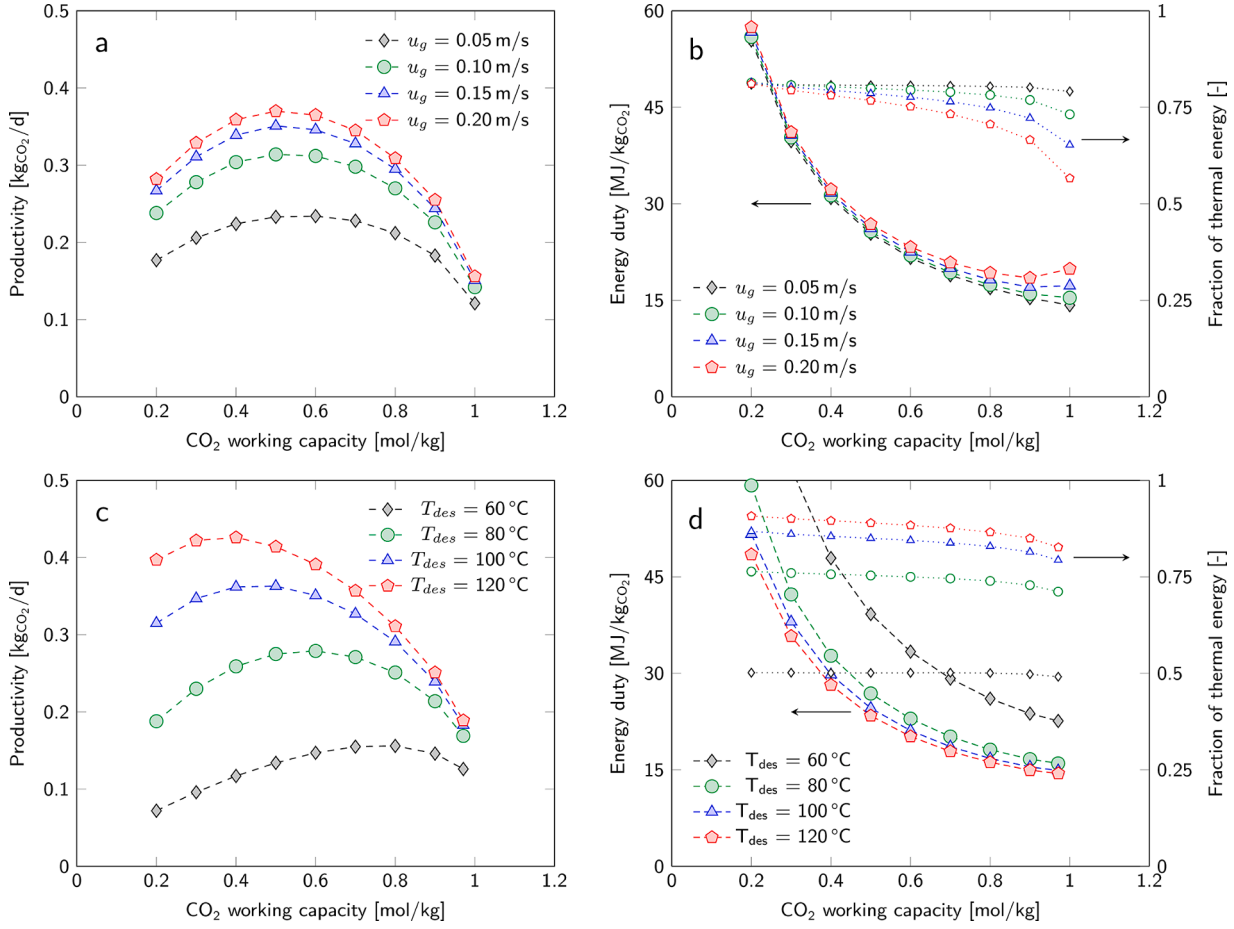

Fig. 6. Two dimensional sensitivity analyses with the effect of working capacity and adsorption gas velocity on (a) daily productivity and (b) energy duty and the effect of working capacity and desorption temperature on (c) daily productivity and (d) energy duty. In the graphs presenting the energy duty, the filled symbols represent the total energy duty and the open symbols represent the fraction thermal energy of this total.

with the sorbent (less than 0.2 s). The average adsorption temperature and relative humidity of the ambient air are 20°C and 70 %, respectively. These are subject to minor fluctuations, since air is extracted from inside the laboratory. Treated air is released back into the laboratory. This leads to a slight decrease in CO_2 concentration of the ingoing air in the early stage of adsorption when the released air is very lean in CO_2. In the simulations, the actual momentary CO_2 inlet concentration is used, since averaging was not sufficient for an accurate description. For the ambient conditions on the other hand, the previously mentioned averages are used in the simulations. The presence of water vapour is known

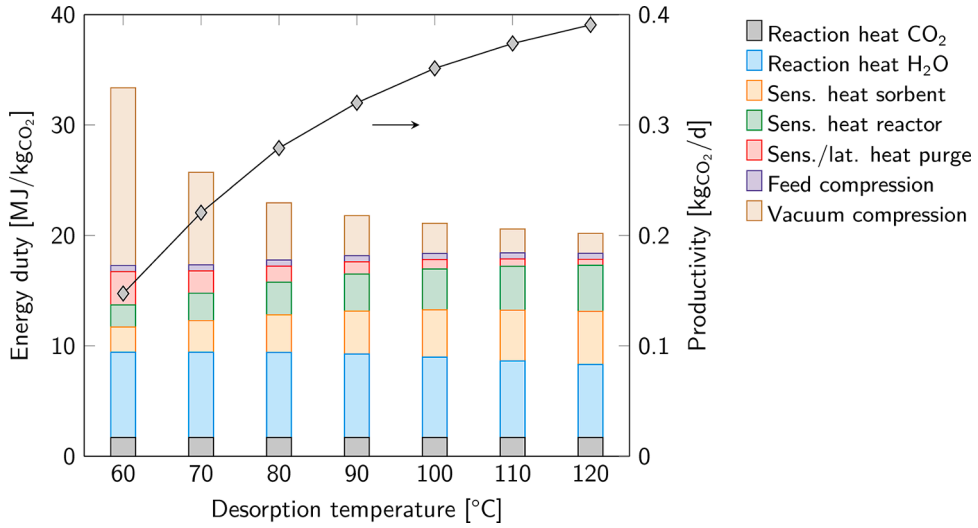

Fig. 7. Distribution of energy consumption as function of desorption temperature for a CO_2 working capacity of 0.6 mol/kg.

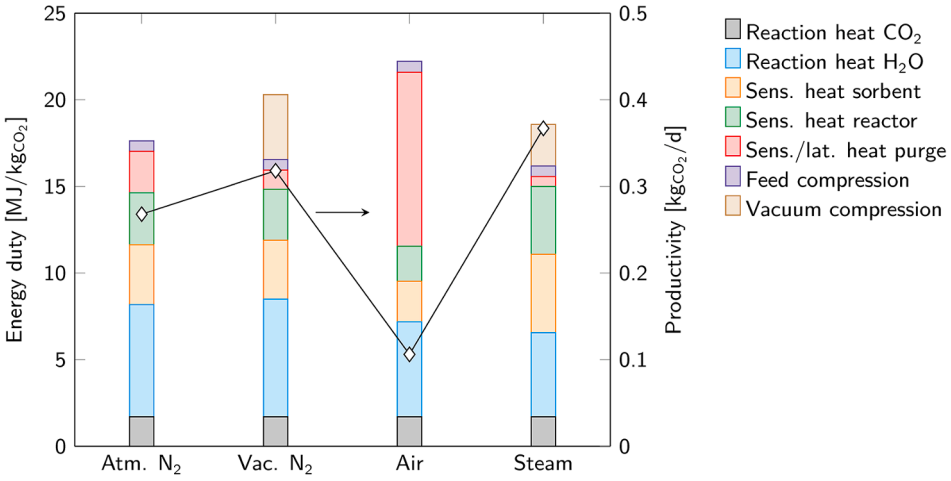

Fig. 8. Distribution of energy requirements and daily productivity for the selected regeneration strategies.

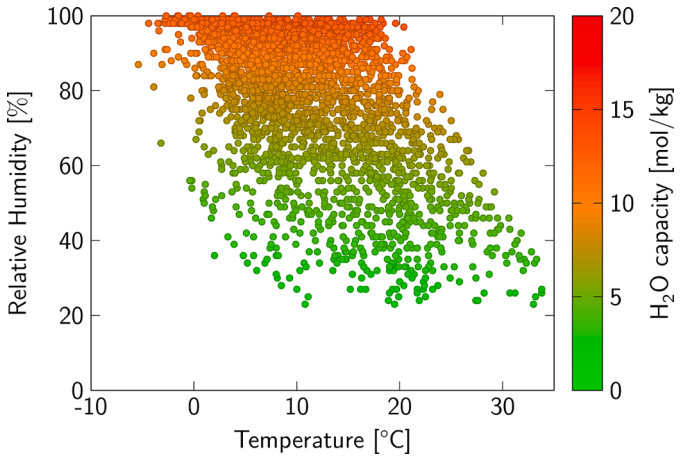

Fig. 9. Occurrences of a combination of temperature and humidity in Enschede, the Netherlands throughout one year (KNMI, 2020). The H_2O equilibrium capacity following the GAB model (Eq. (6)) for each combination of temperature and relative humidity are indicated with the colour map.

to enhance CO_2 adsorption (Veneman et al., 2015; Patel et al., 2017; Wurzbacher et al., 2016; Serna-Guerrero et al., 2008). Therefore, the Tóth isotherm model is extended with a description for the CO_2 equilibrium capacity as function of relative humidity based on literature data from Veneman et al. (2015). The difference between model and experimental results of the CO_2 outlet concentration are within 7% over the entire experiment at a superficial gas velocity of 0.15 m/s (Fig. 4b). For all experiments, the difference between experimental and modelling results remains within 10 %. Here, the absolute difference is normalized by the difference between maximum and minimum measured value (Eq. (13)).

$$Difference(\%) = \frac{y_{\text{model}} - y_{\text{exp}}}{\max(y_{\text{exp}}) - \min(y_{\text{exp}})} \times 100\% \tag{13}$$

For the sorbent loading a maximum difference of 5 % is found. With this, the adsorption model is considered to be accurate in describing this system, especially considering that no fitting parameters are used at all.

During desorption, the CO_2 concentration of the product gas stream is measured. This stream may contain a significant amount of water, which upon condensation could damage the CO_2 analyzer. Therefore, a silica guard bed is installed before the CO_2 concentration is determined. This silica bed also has a small CO_2 capacity, which will introduce some residence time distribution. Consequently, the measured CO_2

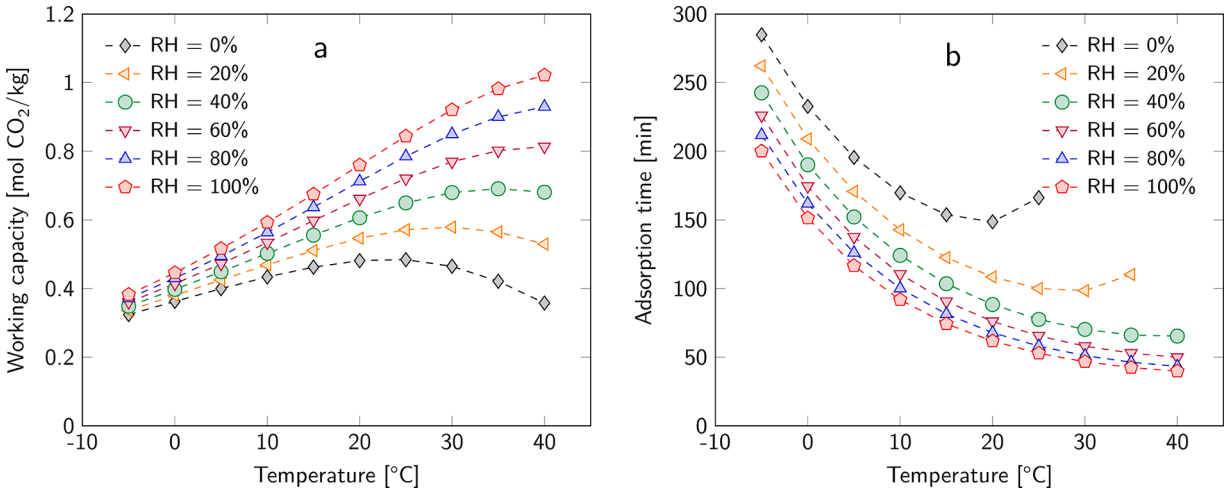

Fig. 10. Effect of weather conditions on (a) working capacity at a constant adsorption time of 90 min and (b) adsorption time at a constant working capacity of 0.6 mol/kg (i.e. an absolute sorbent loading of 0.8 mol/kg).

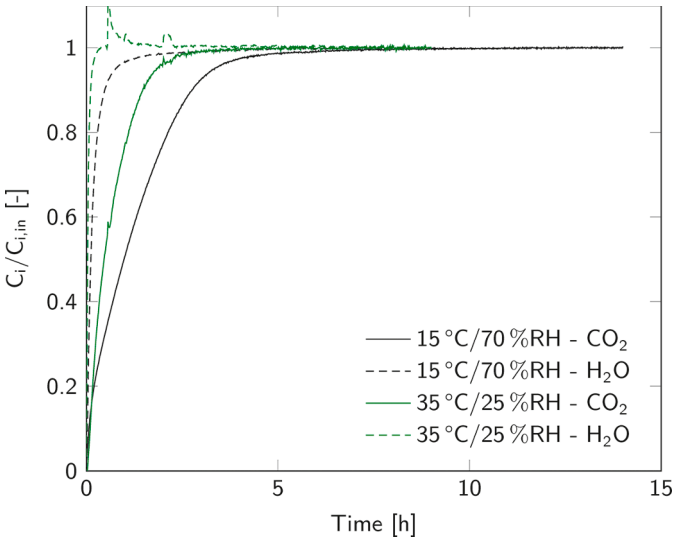

Fig. 11. Breakthrough behaviour of CO_2 and H_2O at two experimental conditions.

concentration will not directly represent the gas stream that leaves the reactor. This means that the outlet CO_2 concentration is not a suitable method for direct model validation. The dynamics of the CO_2 adsorption in the guard bed should then be taken into account. As an alternative, we here use the reactor temperature for validation. Both CO_2 and H_2O desorption are endothermic processes with a significant energy effect and heat transfer through the bed limits the desorption rate. In other words, once the temperature is described correctly, it is inevitable that the desorption behaviour is also described correctly.

Fig. 5a shows the model and experimental results of the temperature for desorption under reduced pressure (350 mbar) with N_2 as purge gas. Initially, the temperature is overestimated by 10 – 20 %, but for the remainder it is accurate within 5 % (Fig. 5b). For desorption at atmospheric pressure, the differences are even smaller. There are a number of possible causes for the overprediction of the bed temperature at the beginning. Firstly, the temperature of the heating medium is assumed constant, whereas in reality this drops when it flows through the bed. This is more significant at the beginning when the heating rate is higher. Secondly, the kinetics of H_2O desorption are unknown, although it is clear that it is faster than the desorption rate of CO_2. It is very well possible that H_2O desorbs faster than assumed in the model, which results in more energy consumption (for H_2O desorption) at the start of a desorption experiment and, hence, a slower temperature increase.

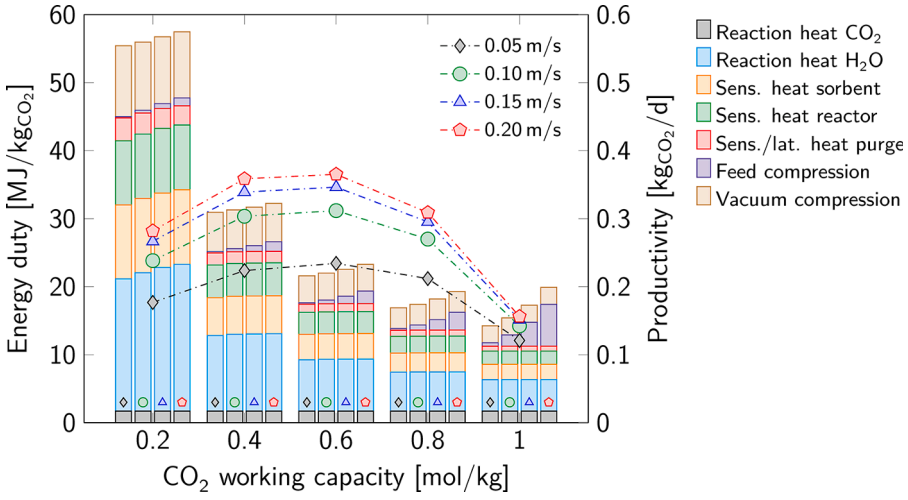

Fig. 12. Sensitivity analysis of varying adsorption superficial gas velocity and CO_2 working capacity. The bars show the distribution of the energy contributors for each working capacity and superficial gas velocity (indicated by the symbols). The lines represent the CO_2 productivity.

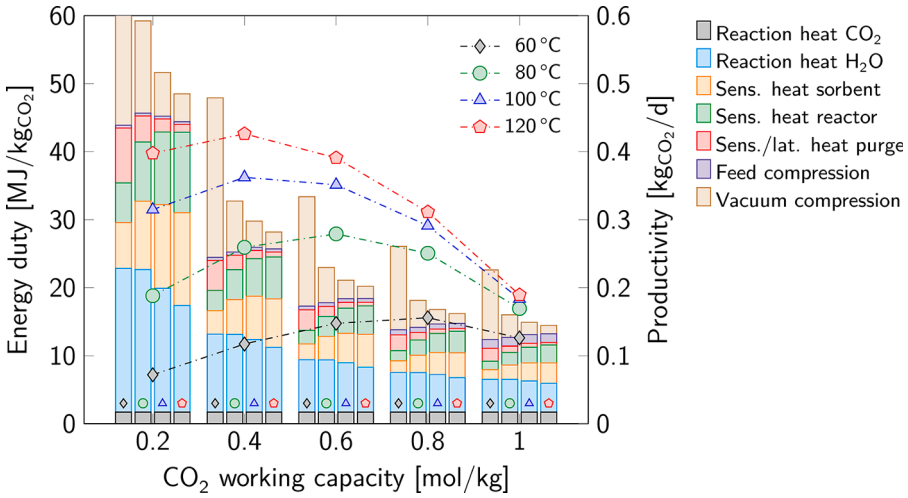

Fig. 13. Sensitivity analysis of varying desorption temperature and CO_2 working capacity. The bars show the distribution of the energy contributors for each working capacity and desorption temperature (indicated by the symbols). The lines represent the CO_2 productivity.

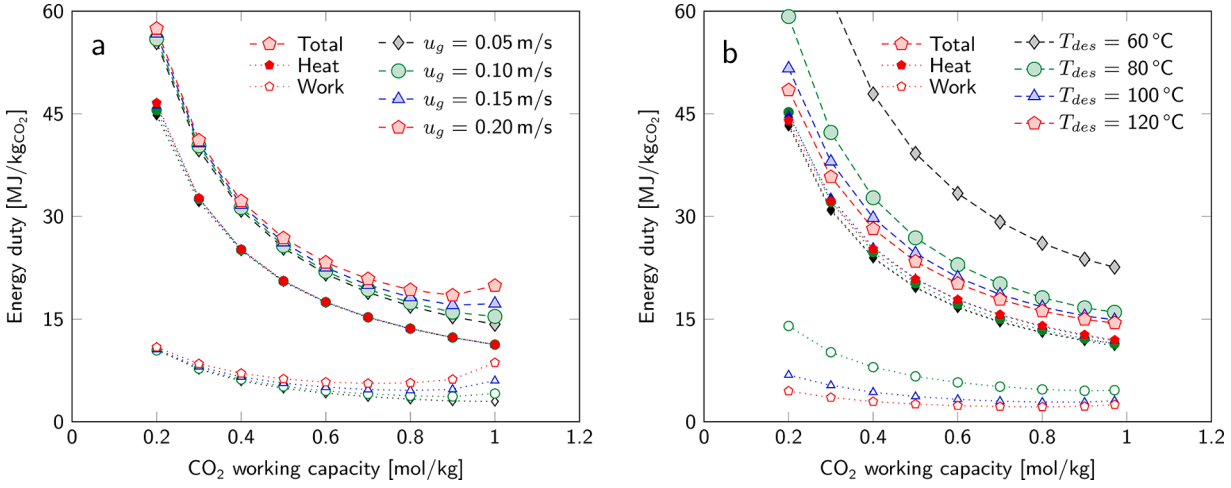

Fig. 14. Energy duty of the sensitivity analyses showing the total energy duty and the amount of thermal energy ('heat') and electrical energy ('work'). Note that for varying desorption temperature, the thermal energy and electrical energy requirements are nearly identical at 60°C.

Finally, the heat transfer coefficient is determined for a stagnant fixed bed at atmospheric conditions. Heat transfer at reduced pressure is slower than at atmospheric pressure, which contributes to the observed differences between model and experimental results. Despite the model improvements that could be made for the initial desorption stage, we consider the desorption model sufficiently accurate for further use in process optimization.

4.2. Sensitivity analyses

Sensitivity analyses show the effect of operational parameters on key performance indicators (KPIs). The complete adsorption-desorption cycle is modelled for three consecutive cycles. Initial calculations showed that this results in a cyclic steady state. This was determined by evaluating the CO_2 loading profile in axial direction of the bed of each consecutive cycle. In all cases, the loading profile of the second and third cycle were nearly identical. Therefore, three cycles will be used as default for all simulations. The KPIs are calculated from the results of the last cycle. Adsorption and desorption continue until a certain average sorbent loading is achieved. The sorbent loading after adsorption is varied as one of the operational parameters in the sensitivity analyses, whereas desorption always ends at an average sorbent loading of 0.2 mol/kg. Deeper regeneration results in a longer, more energy intensive desorption phase, whereas a higher remaining CO_2 loading results in a worse sorbent utilization. The chosen value seems to be a reasonable trade-off, but an optimal value could be determined in a more extensive optimization study. The resulting sorbent working capacity is a measure for the adsorption (and desorption) time, which is of great significance for both CO_2 productivity and energy duty.

A two-dimensional sensitivity analysis is performed using working capacity, and thus adsorption time, and superficial gas velocity during adsorption as variables. Their effect on the KPIs, daily productivity and energy duty, are shown in Fig. 6a and b, respectively. In addition, the energy duty is divided into thermal energy ('heat') and electrical energy ('work'). The fraction of thermal energy is also given in Fig. 6b. Note that these results are obtained for a given sorbent with its adsorption isotherm and a fixed amount of sorbent.

There is an optimal working capacity in terms of productivity (Fig. 6a). This optimum occurs due to heat transfer limitations at low working capacity and due to CO_2 equilibrium capacity limitations towards high working capacity. Heat transfer limitation occurs in the transition between adsorption and desorption. Then, neither adsorption nor desorption takes place, hence it is some sort of downtime of the system. At low working capacity, adsorption and desorption are fast and therefore this downtime is relatively long. Consequently, the productivity decreases towards low working capacity. The productivity will

also decrease towards a higher working capacity. The adsorption rate lowers as adsorption progresses, because it is limited by the CO_2 equilibrium capacity. Adsorption will take longer; hence, fewer cycles per day can be realized. Therefore, the daily productivity will decrease.

Increasing the gas velocity results in a faster adsorption rate, because the average CO_2 concentration throughout the bed will increase. This results in a higher productivity at increasing superficial gas velocity. However, internal mass transfer and/or reaction kinetics then become more dominant and the effect of increasing gas velocity on productivity flattens off. Operating at high working capacity is beneficial in terms of energy duty (Fig. 6b). Fewer cycles are required at increasing working capacity, which reduces the sensible heat requirement. In addition, the energy penalty for water desorption reduces with increasing working capacity. Although the working capacity of CO_2 increases, it does not result in a higher H_2O working capacity, because the sorbent is quickly saturated with the more abundantly available water vapour. In other words; a higher CO_2 working capacity leads to an increase in CO_2 selectivity. On the other hand, an additional energy penalty for feed compression is paid due to increased adsorption time. Therefore, at very high working capacity (or adsorption time) and high gas velocity, the overall energy costs increase again. A more detailed analysis of the energy distribution of this sensitivity analysis is available in Appendix B. Varying superficial gas velocity during adsorption only affects the energy cost for feed compression and, for short adsorption times, also the reaction heat for H_2O desorption at constant working capacity. The former is the result of a higher pressure drop, which is not completely compensated by a shorter adsorption time. The latter only occurs at a very short adsorption time, when the H_2O loading has not yet reached equilibrium. This means that at constant working capacity, the thermal energy requirement is (except at short adsorption time) constant and differences in the fraction of thermal energy are caused by feed compression costs. The superficial gas velocity seems to affect the total energy duty only slightly, however, feed compression costs for a working capacity of 0.6 mol/kg increase by a factor of nine when increasing the gas velocity from 0.05 to 0.2 m/s. This means that feed compression is not a major energy consumer at these conditions. The fraction of required thermal energy emphasizes these observations. Only at high working capacity for high gas velocity, the fraction of electrical energy is rapidly increasing and feed compression becomes significant.

A second two-dimensional sensitivity analysis shows the effect of working capacity and desorption temperature on productivity and energy duty, including the fraction thermal energy (Fig. 6c and d). Both productivity and energy duty take advantage of a higher desorption temperature. It appears that desorption temperature is limited by thermal stability of the sorbent. An important point to note here, is that the reported desorption temperature refers to the temperature of the heating medium and not the temperature of the actual sorbent bed, hence the sorbent bed does not necessarily reach the temperature of the heating medium at the end of desorption. A higher desorption temperature is beneficial for productivity since it reduces desorption time. Furthermore, the optimal working capacity shifts towards a lower value when increasing desorption temperature. Since the heating medium has a higher temperature, the heating phase is shorter and therefore the 'downtime' of the cycle is shorter.

In terms of energy duty, intuitively one would argue that an increase in ΔT from adsorption to desorption would raise the energy duty. The sensible heat requirement is indeed rising with temperature; however, this also reduces desorption time and consequently the compression costs of the purge gas (Fig. 7). Therefore, the fraction of electrical energy is highly reduced at increasing desorption temperature (Fig. 6d). A trend that is valid throughout the whole range of working capacity as shown in Fig. 13 in Appendix B.

From these sensitivity analyses we can conclude that desorption temperature is preferably high, and probably limited by sorbent stability. Also, the adsorption gas velocity has a limited influence on energy duty, but does increase productivity up to a gas velocity of 0.15 m/s. After this, internal mass transfer and reaction kinetics are limiting the adsorption rate. Furthermore we can conclude that a complete optimization is not possible based solely on these analyses. A trade-off between productivity and energy consumption is required, which should then be optimized towards total cost of capture. Moreover, these sensitivity analyses only provide a two-dimensional view, whereas a complete optimization has much more dimensions.

As an example, let's consider the option of desorption at low temperature for a constant working capacity of 0.6 mol/kg. Fig. 7 shows that this is very energy intensive, where most of the energy (besides the unavoidable heats of desorption) is spent on purge gas heating and vacuum compression. At this lower temperature, desorption kinetics may be limiting instead of equilibrium capacity. Which raises the question whether it is required to operate at reduced pressure and the current purge gas flow. These parameters together with the initial sorbent loading (0.2 mol/kg is used in all of these simulations) are not evaluated. Therefore, this multi-dimensional problem requires a much more detailed optimization study combined with economic analysis to find the optimal, case specific operational parameters.

4.3. Desorption options

Desorption with an inert purge gas (as e.g. nitrogen, applied in experiments in the present work) is useful for laboratory testing purposes, however it has two disadvantages in large scale applications. Firstly, introducing a purge gas dilutes the product gas. A purge gas reduces the partial pressure of CO_2 during desorption and therefore enhances the desorption rate. However, utilization strategies often require pure CO_2 (e.g. for chemical reduction). A condensable purge gas, such as steam, resolves this issue, but comes on its term with additional costs to produce the purge gas by evaporation. When using steam, a reduced pressure is probably required, since the major part of desorption will operate below the boiling point at atmospheric pressure. Secondly, the use of a non-condensable purge gas raises the question where this purge gas (e.g. nitrogen) is obtained. From a sustainability (and economic) point of view, the use of an unrecoverable purge gas is unfavorable. An exception can be the use of ambient air, when a diluted product stream (1 – 5 %) is not a problem. Moreover, this is even a frequently used option for CO_2 supply in various horticulture applications and for microalgae cultivation. However, when using air in combination with the current sorbent, the desorption temperature is limited to 70°C to avoid rapid oxidative degradation.

We evaluated these alternative desorption methods to show that they are possible with a similar energy consumption compared to desorption with a nitrogen purge (Fig. 8). The evaluated desorption methods include: a nitrogen purge at atmospheric pressure, a nitrogen purge at reduced pressure (350 mbar), an air purge at atmospheric pressure and a steam purge at reduced pressure (100 mbar). The operating conditions are based on the sensitivity analyses, however they are not necessarily optimized. Adsorption conditions are the same for all simulations (P_{CO2} = 41 Pa, T = 20°C, RH = 50 %, Δq = 0.7 mol/kg, u_g = 0.1 m/s). Desorption temperature depends on the purge gas: 90°C for nitrogen, 70°C for air and 120°C for steam. For steam, the purge flow is set at 1 NL/min, where for the other cases this is 20 NL/min.

Vacuum desorption is faster than atmospheric desorption, causing an increase in productivity and reducing the sensible heat demand of the purge gas. However, the energy penalty to achieve vacuum is significant and causes the total energy consumption to be higher. The choice whether to use vacuum or not likely depends on the purge gas flowrate and desorption pressure. Also regarding these considerations, a multi-dimensional optimization study is necessary to provide these insights and to quantify the costs.

Using an air purge leads to the lowest productivity at the highest energy costs. The desorption step takes a long time, mainly due to the lower desorption temperature and consequently a slower heating rate. Therefore, purge gas sensible heat becomes the largest cost driver.

Reducing desorption time by lowering the working capacity will not be a good alternative. Since the sensitivity analysis (Fig. 6c and d) show that $\Delta q = 0.7$ mol/kg is already close to maximum productivity and the energy consumption will only rise when reducing the working capacity. Reducing purge gas flow rate could be beneficial, since, also with air, the desorption rate is limiting and not the equilibrium loading. However, this will slightly reduce the productivity, which is already low. From an economic point of view, air as purge gas offers several advantages. First of all, it is free of costs and abundantly available. Secondly, it results in a simpler process design, especially for desorption at atmospheric conditions. Finally, the lower desorption temperature provides more opportunities to use waste heat as energy source.

Steam desorption is an interesting alternative showing the highest productivity. However, to reach a comparable energy consumption, desorption conditions with a steam purge are much harsher than for the nitrogen purge. Sensible heat requirements are a bit higher than for the other options, due to the higher desorption temperature. The high productivity means that the desorption rate at these conditions is faster than with the nitrogen purge. This means that purge gas flowrate, which differs by a factor of 20, does not affect productivity very much at a high temperature.

In conclusion, for these different regeneration options at constant working capacity, the differences in productivity are more pronounced than the differences in energy consumption.

4.4. Influence of weather conditions

Standard adsorption conditions in the simulations for optimization were 20°C and 50 % RH. Also in literature, these conditions were often used to design and optimize DAC processes (Keith et al., 2018; Stampi-Bombelli et al., 2020). This is arguably valid for indoor experiments or weather conditions during the day. However, for DAC processes to run day and night throughout the year, these conditions are far from standard. Fig. 9 shows the occurrences of a combination of relative humidity and temperature within one year (01/11/19 – 01/11/20) in Enschede, The Netherlands (KNMI, 2020). The relative humidity is generally high. Furthermore, high temperature is usually combined with a low relative humidity, whereas the relative humidity is high at low temperature. Overall, it becomes clear that the chosen conditions (20°C and 50 % RH) are not a valid representation of the actual ambient conditions. In fact, the average temperature and relative humidity are 11°C and 77 %, respectively.

An average annual temperature and relative humidity will also not be representative for the system throughout the year. Important factors for productivity and energy duty, such as adsorption equilibrium capacity and reaction kinetics, have a nonlinear relation with respect to temperature and/or relative humidity. Also, sensible heat requirements to reach desorption temperature are affected. Furthermore, H_2O co-adsorption already causes a significant energy penalty at 20°C and 50 % RH, as indicated in the energy consumption distribution in Figs. 7 and 8. Fig. 9 illustrates the H_2O equilibrium capacity (Eq. (6)) for all combinations of temperature and relative humidity. It becomes clear that H_2O co-adsorption will become even more significant at the average conditions identified above.

The effects of reaction kinetics and CO_2 equilibrium capacity are assessed using the adsorption fixed bed model. Again, the model is extended with a description of the CO_2 capacity enhancement due to H_2O co-adsorption. The initial CO_2 loading (i.e. CO_2 loading after desorption) is 0.2 mol/kg in all simulations, the gas velocity is 0.3 m/s and the CO_2 partial pressure is 41 Pa. The high gas velocity eliminates potential external mass transfer limitations. Two sets of simulations are performed in a temperature range of -5°C to 40°C and relative humidity over the full range. First, the CO_2 working capacity is determined after 90 min of adsorption (Fig. 10a) and second, the adsorption time is determined to reach a working capacity of 0.6 mol/kg (Fig. 10b).

The slowest adsorption rate occurs at low temperature, even though the CO_2 equilibrium capacity is the highest. This means that, at low temperature, adsorption is clearly limited by reaction kinetics. This is also the reason that the effect of relative humidity on the working capacity is relatively small at low temperature (Fig. 10a). Reaction kinetics become faster as the temperature increases, which results in more adsorption after a fixed amount of time. However, at increasing temperature, the CO_2 equilibrium capacity decreases. Therefore, at high temperature, the driving force for adsorption will decrease and thus the adsorption rate. At high humidity, this limitation is less pronounced due to the enhancement of CO_2 equilibrium capacity; hence, limitation in adsorption rate will occur at a higher temperature. The same phenomena lead to the trends observed in Fig. 10b. Here, it shows the time it takes until a CO_2 working capacity of 0.6 mol/kg is reached, which is an absolute CO_2 sorbent loading of 0.8 mol/kg. The limitation in driving force at high temperature and low humidity is evident. At these conditions, (e.g. 40°C and 0 % RH) the equilibrium capacity is lower than 0.8 mol/kg and it is not possible to reach the desired working capacity.

The available experimental dataset for CO_2/H_2O co-adsorption is still limited and, for this study, required extrapolation towards higher humidity and the temperature extremes. Especially at high humidity and high temperature, the enhancement is likely to be overestimated. An extension of the dataset and a detailed mechanistic study is required to make an accurate assessment of the impact of weather conditions on the adsorption process.

Overall, there is a large spread in the adsorption rate at different weather conditions. Therefore, productivity and energy duty will also greatly depend on weather conditions. However, this is not reflected in design studies assuming moderate or averaged operating conditions. Most likely this results in overestimating productivity and underestimating the energy costs for a continuous production of CO_2 from air. In addition, optimal operating conditions will differ throughout the seasons and even between day and nighttime. In that case, most likely dynamic control of the operating parameters is required for the most efficient adsorption process.

5. Conclusion

This study discussed an optimization strategy of a kg-scale adsorption-based DAC system. The system was modelled incorporating mass- and heat transfer on particle and bed level and validated by experimental data. Sensitivity analyses showed that desorption temperature should be as high as possible, hence, limited by sorbent stability. Furthermore, gas velocity during adsorption does not have a large impact on energy duty, but does significantly affect productivity. Finally, working at a high working capacity limits the productivity of the process, however it is beneficial in terms of energy requirement. Such trade-off between productivity and energy duty can only be assessed with a more detailed multi-dimensional optimization study combined with an economical assessment.

The location of DAC is an important factor in process optimization. Firstly, weather conditions and diurnal variations significantly affect process performance and therefore the optimal operation parameters. Furthermore, despite of all optimization efforts, DAC remains an energy intensive process. Availability of low cost energy (e.g. waste heat, low-grade steam) will therefore be important for the viability of DAC. Finally, economic viability is also determined by the sales price of CO_2, which can vary significantly with the location.

Overall, this study provides a clear insight in the effects of weather conditions and operating conditions on energy consumption and system productivity. With these insights and the developed model, it provides a sound basis for further process development and optimization of DAC using fixed bed technology combined with solid amine sorbents.

Declaration of Competing Interest

The authors declare that they have no known competing financial

interests or personal relationships that could have appeared to influence the work reported in this paper.

Acknowledgement

This research was funded by NORTH-WEST EUROPE INTERREG, grant number NWE 639 as part of the IDEA project (Implementation and development of economic viable algae-based value chains in North-West Europe). Benno Knaken, Johan F.H. Agterhorst, and Ronald A. Borst (Sustainable Process Technology group, University of Twente) are acknowledged for their invaluable efforts and skills in the construction of the reactor.

Appendix A. H_2O/CO_2 breakthrough experiments

Breakthrough experiments of combined H_2O and CO_2 adsorption show that adsorption of H_2O is much faster than adsorption of CO_2. These experiments are performed in the same fixed bed reactor as the CO_2 breakthrough experiments (Section 2.2). Here, some part of the N_2 is first saturated with H_2O to achieve the desired relative humidity. Fig. 11 shows the concentration of the species in the gas that leaves the reactor normalized to the concentration that enters the reactor. It shows, for two experimental conditions, that equilibrium of H_2O adsorption is reached much earlier than equilibrium of CO_2 adsorption. The time it takes to reach 99 % of the inlet concentration is two times faster for H_2O than for CO_2 for adsorption at 15°C and 70 % RH and nine times faster for adsorption at 35°C and 25 % RH. The assumption that the sorbent is much faster saturated with H_2O than with CO_2 is therefore justified.

Appendix B. Detailed sensitivity analyses

The sensitivity analyses presented in Section 4.2 show only show the total energy duty, fraction of thermal energy and daily productivity. Here, we provide the total breakdown of the energy costs. In these analyses, thermal energy includes:

- reaction heat of CO_2;
- reaction heat of H_2O;
- sensible heat of the sorbent;
- sensible heat of the reactor;
- sensible heat of the purge gas;
- and, in the case of a steam purge, latent heat of the purge gas,

and electrical energy includes:

- compression of the feed (air);
- and compression of purge gas during vacuum desorption.

Fig. 12 shows the detailed sensitivity analysis for varying superficial gas velocity during adsorption and varying working capacity. It combines Fig. 6a and b and shows the distribution of energy contributors. The listed energy contributions are shown in the bar graphs for different superficial velocities, indicated by the symbols in the bottom of the bar graph, and selected CO_2 working capacities. The lines show the corresponding productivity for each of the superficial gas velocities. Fig. 13 combines Fig. 6c and d to shows the detailed sensitivity analysis for varying desorption temperature and varying working capacity.

The fraction of thermal energy is already included in Fig. 6. This does not show the absolute energy consumption by these two types of energy. Therefore, Fig. 14 shows the total energy duty as well as the amount of thermal and electrical energy that is required.

References

Alesi, W.R., Kitchin, J.R., 2012. Evaluation of a primary amine-functionalized ion-exchange resin for CO_2 capture. Ind. Eng. Chem. Res. 51 (19), 6907–6915. https://doi.org/10.1021/ie300452c.

Bajamundi, C.J.E., et al., 2019. Capturing CO_2 from air: technical performance and process control improvement. J. CO2 Util. 30, 232–239. https://doi.org/10.1016/j.jcou.2019.02.002.

Beuttler, C., Charles, L., Wurzbacher, J., 2019. The role of direct air capture in mitigation of anthropogenic greenhouse gas emissions. Front. Clim. 1 (10) https://doi.org/10.3389/fclim.2019.00010.

Bos, M.J., et al., 2019a. Study on transport phenomena and intrinsic kinetics for CO_2 adsorption in solid amine sorbent. Chem. Eng. J. 377, 120374 https://doi.org/10.1016/j.cej.2018.11.072.

Bos, M.J., Kersten, S.R.A., Brilman, D.W.F., 2020. Wind power to methanol: renewable methanol production using electricity, electrolysis of water and CO_2 air capture. Appl. Energy 264, 114672. https://doi.org/10.1016/j.apenergy.2020.114672.

Bos, M.J., Pietersen, S., Brilman, D.W.F., 2019b. Production of high purity CO_2 from air using solid amine sorbents. Chem. Eng. Sci. 2, 100020 https://doi.org/10.1016/j.cesx.2019.100020.

Breyer, C., et al., 2019. Direct air capture of CO_2: a key technology for ambitious climate change mitigation. Joule 3 (9), 2053–2057. https://doi.org/10.1016/j.joule.2019.08.010.

Choi, S., Drese, J.H., Jones, C.W., 2009. Adsorbent materials for carbon dioxide capture from large anthropogenic point sources. ChemSusChem 2 (9), 796–854. https://doi.org/10.1002/cssc.200900036.

D'Alessandro, D.M., Smit, B., Long, J.R., 2010. Carbon dioxide capture: Prospects for new materials. Angew. Chem.-Int. Ed. 49 (35), 6058–6082. https://doi.org/10.1002/anie.201000431.

Driessen, R.T., et al., 2020a. Design and proof of concept of a continuous pressurized multi-stage fluidized bed setup for deep sour gas removal using adsorption. Powder Technol. 366, 859–872. https://doi.org/10.1016/j.powtec.2020.03.013.

Driessen, R.T., Kersten, S.R.A., Brilman, D.W.F., 2020b. A thiele modulus approach for nonequilibrium adsorption processes and its application to CO_2 capture. Ind. Eng. Chem. Res. 59 (15), 6874–6885. https://doi.org/10.1021/acs.iecr.9b05503.

Duong, D.D., 1998. Adsorption Analysis: Equilibria and Kinetics. Series on Chemical Engineering. Imperial College Press, London v. 2; Series on chemical engineering; v. 2.

Elfving, J., et al., 2021. Experimental comparison of regeneration methods for CO_2 concentration from air using amine-based adsorbent. Chem. Eng. J. 404, 126337 https://doi.org/10.1016/j.cej.2020.126337.

Fasihi, M., Efimova, O., Breyer, C., 2019. Techno-economic assessment of CO_2 direct air capture plants. J. Cleaner Prod. 224, 957–980. https://doi.org/10.1016/j.jclepro.2019.03.086.

Froment, G.F., Bischoff, K.B., De Wilde, J., 2011. Chemical Reactor Analysis and Design, third ed. John Wiley & Sons, Inc, Hoboken, NJ.

Gebald, C., et al., 2011. Amine-based nanofibrillated cellulose as adsorbent for CO_2 capture from air. Environ. Sci. Technol. 45 (20), 9101–9108. https://doi.org/10.1021/es202223p.

Gelles, T., et al., 2020. Recent advances in development of amine functionalized adsorbents for CO_2 capture. Adsorption 26 (1), 5–50. https://doi.org/10.1007/s10450-019-00151-0.

Glueckauf, E., Coates, J.I., 1947. 241. Theory of chromatography. Part IV. The influence of incomplete equilibrium on the front boundary of chromatograms and on the effectiveness of separation. J. Chem. Soc. (0), 1315–1321. https://doi.org/10.1039/JR9470001315.

Goeppert, A., et al., 2012. Air as the renewable carbon source of the future: an overview of CO_2 capture from the atmosphere. Energy Environ. Sci. 5 (7), 7833–7853. https://doi.org/10.1039/C2EE21586A.

Keith, D.W., et al., 2018. A process for capturing CO_2 from the atmosphere. Joule 2 (8), 1573–1594. https://doi.org/10.1016/j.joule.2018.05.006.

KNMI, Uurgegevens van het weer in Nederland, 2020 cited: 11-11-2020, Available from: http://projects.knmi.nl/klimatologie/uurgegevens/selectie.cgi.

Lackner, K.S., et al., 2012. The urgency of the development of CO_2 capture from ambient air. Proc. Natl. Acad. Sci. 109 (33), 13156–13162. https://doi.org/10.1073/pnas.1108765109.

Lackner, K.S., Ziock, H.-J., Grimes, P., 1999. Carbon dioxide extraction from air: is is an option?. In: 24th Annual Technical Conference on Coal Utilization. DOI.

Lim, X., 2015. How to make the most of carbon dioxide. Nature 526, 628–630. https://doi.org/10.1038/526628a.

Patel, H.A., Byun, J., Yavuz, C.T., 2017. Carbon dioxide capture adsorbents: chemistry and methods. ChemSusChem 10 (7), 1303–1317. https://doi.org/10.1002/cssc.201601545.

Peters, M., et al., 2011. Chemical technologies for exploiting and recycling carbon dioxide into the value chain. ChemSusChem 4 (9), 1216–1240. https://doi.org/10.1002/cssc.201000447.

Quirijns, E.J., et al., 2005. Sorption isotherms, GAB parameters and isosteric heat of sorption. J. Sci. Food Agric. 85 (11), 1805–1814. https://doi.org/10.1002/jsfa.2140.

Rogelj, J., et al., 2015. Energy system transformations for limiting end-of-century warming to below 1.5°C. Nat. Clim. Change 5, 519. https://doi.org/10.1038/nclimate2572 https://www.nature.com/articles/nclimate2572#supplementary-information.

Sanz-Pérez, E.S., et al., 2016. Direct capture of CO_2 from ambient air. Chem. Rev. 116 (19), 11840–11876. https://doi.org/10.1021/acs.chemrev.6b00173.

Schellevis, M., Jacobs, T., Brilman, W., 2020. CO_2 capture from air in a radial flow contactor: batch or continuous operation? Front. Chem. Eng. 2 (19) https://doi.org/10.3389/fceng.2020.596555.

Serna-Guerrero, R., Da'na, E., Sayari, A., 2008. New insights into the interactions of CO_2 with amine-functionalized silica. Ind. Eng. Chem. Res. 47 (23), 9406–9412. https://doi.org/10.1021/ie801186g.

Singh, G., et al., 2020. Emerging trends in porous materials for CO_2 capture and conversion. Chem. Soc. Rev. 49 (13), 4360–4404. https://doi.org/10.1039/d0cs00075b.

Socolow, R., et al., 2011. Direct Air Capture of CO2 with Chemicals: a Technology Assessment for the APS Panel on Public Affairs. American Physical Society.

Sonnleitner, E., Schöny, G., Hofbauer, H., 2018. Assessment of zeolite 13X and Lewatit® VP OC 1065 for application in a continuous temperature swing adsorption process for biogas upgrading. Biomass Convers. Biorefinery 8 (2), 379–395. https://doi.org/10.1007/s13399-017-0293-3.

Speight, J.G., 2011. Chapter 12 - petrochemicals. In: Speight, J.G. (Ed.), Handbook of Industrial Hydrocarbon Processes. Gulf Professional Publishing, Boston, pp. 429–466. , Editor.

Stampi-Bombelli, V., van der Spek, M., Mazzotti, M., 2020. Analysis of direct capture of $ ${\hbox {CO}}_{2}$$CO2from ambient air via steam-assisted temperature–vacuum swing adsorption. Adsorption 26 (7), 1183–1197. https://doi.org/10.1007/s10450-020-00249-w.

Thiele, E.W., 1939. Relation between catalytic activity and size of particle. Ind. Eng. Chem. 31 (7), 916–920. https://doi.org/10.1021/ie50355a027.

Veneman, R., et al., 2012. Continuous CO_2 capture in a circulating fluidized bed using supported amine sorbents. Chem. Eng. J. 207-208, 18–26. https://doi.org/10.1016/j.cej.2012.06.100.

Veneman, R., et al., 2015. Adsorption of H_2O and CO_2 on supported amine sorbents. Int. J. Greenh. Gas Control 41, 268–275. https://doi.org/10.1016/j.ijggc.2015.07.014.

Wijffels, R.H., Barbosa, M.J., Eppink, M.H.M., 2010. Microalgae for the production of bulk chemicals and biofuels. Biofuels Bioprod. Biorefin. 4 (3), 287–295. https://doi.org/10.1002/bbb.215.

Wurzbacher, J.A., et al., 2016. Heat and mass transfer of temperature–vacuum swing desorption for CO_2 capture from air. Chem. Eng. J. 283, 1329–1338. https://doi.org/10.1016/j.cej.2015.08.035.

Yu, Q., et al., 2017. Stability of a benzyl amine based CO_2 capture adsorbent in view of regeneration strategies. Ind. Eng. Chem. Res. 56 (12), 3259–3269. https://doi.org/10.1021/acs.iecr.6b04645.

Yu, Q., Brilman, D.W.F., 2017. Design strategy for CO_2 adsorption from ambient air using a supported amine based sorbent in a fixed bed reactor. Energy Procedia 114, 6102–6114. https://doi.org/10.1016/j.egypro.2017.03.1747.

Yu, Q., Brilman, W., 2020. A radial flow contactor for ambient air CO_2 capture. Appl. Sci. 10 (3) https://doi.org/10.3390/app10031080.

Zeman, F., 2007. Energy and material balance of CO_2 capture from ambient air. Environ. Sci. Technol. 41 (21), 7558–7563. https://doi.org/10.1021/es070874m.